Deexcitation of the complete fusion nucleus ^{155}Tb

Kenton J. Moody
Lawrence Livermore National Laboratory, Livermore, California 94550

James J. Hogan
Department of Chemistry, McGill University, Montreal, Quebec, Canada H3A 2K6
(Received 23 December 1985)

We measured excitation functions for several products of the complete fusion of ^{22}Ne and ^{133}Cs. The compound nucleus, ^{155}Tb, was produced with six excitation energies between 50 and 100 MeV. The experimental data can be well reproduced with an evaporation code which addresses the problem of particle emission at high angular momentum. The production of high-spin isomeric species is favored over the production of low-spin species. We introduce a new computer code which reproduces the trend of the isomer ratios with reaction energy. However, a lack of detailed knowledge of the nuclear levels near the high-spin isomers prevents any great accuracy.

I. INTRODUCTION

In reactions of "light" heavy ions ($A \leq 40$) with medium-mass targets at energies near the nominal Coulomb barrier, the formation of a complete fusion nucleus is an important component of the reaction cross section.[1,2] The decay of this compound nucleus can be described[3–10] either by the sequential statistical emission of particles and gamma rays, or by fission. The fractional probability of depopulation of a given state by the emission of a given particle or photon is determined by the level densities of the daughter nuclei and the transmission coefficients of the evaporated particles, both of which are functions of excitation energy, angular momentum, and deformation of the nucleus as a whole.[10] At excitation energies in excess of one neutron binding energy over the yrast line in systems where fission is not important, neutron emission dominates. However, in heavy-ion reactions, large angular momenta can be produced in the compound nuclei, resulting in increased deformation and an enhanced probability of alpha particle emission.[10]

The measurement of products arising from the evaporation of alpha particles and the determination of isomer ratios provide a means of probing our understanding of the evolution of excitation energy—angular momentum (E-J) populations in highly deformed nuclei as particles are emitted. Emission of the heavy alpha particle can remove more angular momentum than can neutron and proton emissions. The population of different isomeric states is strongly dependent on the E-J distributions near the yrast line, and also on the structure of discrete states near the isomers.[11–14]

We have measured the cross sections for several of the products of the complete fusion of ^{22}Ne with ^{133}Cs; we have produced the ^{155}Tb compound nucleus with six different excitation energies between 50 and 100 MeV. We chose this system for several reasons: (1) Fission plays only a small role in the deexcitation process at the highest energy we studied.[15] (2) Many of the nuclides resulting from multiple neutron evaporation exist in more than one isomeric state.[16] (3) The products of deexcitation by emission of one alpha particle and several neutrons have been produced in other heavy-ion work via the formation of the ^{151}Eu compound nucleus followed by neutron evaporation.[17,18] (4) It has been shown in other work that the terbium reaction products are readily observable.[19]

In this work, we have tried to reproduce our cross-section data with the Hauser-Feshbach evaporation code ALERT,[10] and have attempted to calculate the isomer ratios of the terbium isotopes with a second computer code, described herein, from the output E-J distributions.

II. EXPERIMENT

Targets used in these experiments consisted of ~ 600 μg/cm^2 CsCl, vacuum-evaporated in a 1.9-cm-diam spot on backings of 100 mg/cm^2 Au or 40 mg/cm^2 Ni, both of which are sufficiently thick to stop the full energy beam.[20,21] Gold-backed targets had a 75 μg/cm^2 Au layer evaporated over the CsCl to reduce sputtering losses during the irradiations; the nickel-backed targets had a similar 70 μg/cm^2 Ni cover.

We directly water-cooled the targets during irradiation. They acted as the beam stop of a Faraday cup through a vacuum seal. A magnet suppressed the electrons between the target and the 1.6-cm-diam collimator. An integrating electrometer measured the beam current throughout the irradiations. We recorded the integral periodically to allow for the construction of irradiation histories for subsequent cross-section calculations.

We performed these irradiations at the Lawrence Berkeley Laboratory's 88-in. cyclotron, which delivered beams of 94 and 104 MeV ^{22}Ne^{4+}, and 115, 125, 136, and 146 MeV ^{22}Ne^{5+} to the targets. Beam intensities were typically between 0.5 and 1.2 electrical microamperes. The cover layers of gold and nickel, and the CsCl layers themselves, degraded the beam energy by 1.0 MeV (for 146 MeV ^{22}Ne) to 1.4 MeV (for 94 MeV ^{22}Ne) before reaching the center of the target material.[20,21] Products arising from fusion reactions recoiled in the beam direc-

TABLE I. Decay data used in cross-section calculations.

Nuclide	J^π	Half-life	Decay mode	Representative gamma rays (keV)	
^{152}Tb	2^-	17.5±0.1 h	100% EC, β^+	271.1	(7.9%)
				344.3	(57.0%)
				586.3	(8.2%)
				778.9	(5.0%)
^{152}Tb^m	(8^+)	4.3±0.1 min	(79±1)% IT	159.6	(16.5%)
			(21±1)% EC, β^+	283.3	(58.7%)
				344.3	(20.1%)
				411.1	(18.1%)
^{151}Tb	$\frac{1}{2}^+$	17.6±0.1 h	99 + % EC, β^+	108.3	(25%)
			0.01% α	251.7	(26%)
				287.0	(25%)
				479.0	(16%)
^{151}Tb^m	$\frac{11}{2}^-$	25 s	93% IT	(not observed)	
			7% EC, β^+		
^{150}Tb^A	2^-	3.5±0.1 h	100% EC, β^+	496.3	(14.9%)
				638.0	(72.3%)
				650.4	(4.1%)
				792.5	(4.4%)
^{150}Tb^B	(9^+)	6.0±0.2 min	100% EC, β^+	438.4	(41.7%)
				638.0	(99.2%)
				650.4	(69.4%)
				827.5	(40.7%)
^{149}Tb	$(\frac{1}{2}^+)$	4.15±0.03 h	(84±1)% EC, β^+	352.2	(29.7%)
			(16±1)% α	388.6	(18.6%)
				652.1	(16.4%)
				853.4	(15.6%)
^{149}Tb^m	$(\frac{11}{2}^-)$	4.16±0.04 min	99 + % EC, β^+	165.0	(6.9%)
			0.02% α	630.7	(2.6%)
				796.0	(92.0%)
^{148}Tb	2^-	60 min	100% EC, β^+	784.5, 1078.1 (not observed)	
^{148}Tb^m	(9^+)	2.20±0.05 min	100% EC, β^+	394.5	(85.6%)
				631.9	(94.5%)
				784.5	(99.5%)
				882.4	(91.5%)
^{147}Tb	$(\frac{5}{2}^+)$	1.65 h	100% EC, β^+	694.4, 1152.2 (not observed)	
^{147}Tb^m	$(\frac{11}{2}^-)$	1.83±0.06 min	100% EC, β^+	1178.9	(2.0%)
				1397.7	(83.2%)
				1797.8	(13.9%)
^{146}Tb	1^+ and 4^-	8 and 23 s	100% EC, β^+	(observed via daughter and granddaughter)	
^{148}Gd	0^+	74.6 yr	100% α		
^{147}Gd	$\frac{7}{2}^-$	38.1±0.1 h	100% EC, β^+	229.3	(64.4%)
				369.9	(16.6%)
				396.0	(34.1%)
				928.9	(18.8%)
^{146}Gd	0^+	48.3±0.1 days	100% EC, β^+	(observed via daughter)	

TABLE I. (*Continued*).

Nuclide	J^π	Half-life	Decay mode	Representative gamma rays (keV)	
^{145}Gd	$\frac{1}{2}^+$	23±1 min	100% EC, β^+	1757.9	(34.2%)
				1880.6	(32.6%)
^{148}Eu	5^-	55.6±0.2 days	100% EC, β^+	550.3	(99.0%)
				553.2	(17.1%)
				611.3	(19.3%)
				629.9	(70.9%)
^{147}Eu	$\frac{5}{2}^+$	24.6±0.1 days	100% EC, β^+	121.3	(22.7%)
				197.3	(25.8%)
				677.6	(10.7%)
				1077.2	(6.4%)
^{146}Eu	4^-	4.51±0.03 days	100% EC, β^+	634	(80%)
				747.2	(98%)
				901.0	(9.4%)
				1058.7	(6.7%)
^{145}Eu	$\frac{5}{2}^+$	5.93±0.04 days	100% EC, β^+	653.5	(15.3%)
				893.7	(65.8%)
				1658.7	(16.5%)
				1997.0	(7.0%)

tion and were stopped in the thick backing foils.

We irradiated two targets at each projectile energy, one backed with nickel and one with gold. The nickel-backed targets were irradiated for 3—6 h. After the end of each irradiation, we cut the beam spot from the center of the target to reduce the mass of nickel. We then dissolved the beam spot under partial vacuum in 3 ml fuming nitric acid containing a known aliquot of ^{153}Gd tracer and 2.5 mg of lanthanum carrier. The added ^{153}Gd activity was 3 orders of magnitude more intense than that which could be expected as a reaction product. After dissolution, we boiled the solution then diluted it to a volume of 8 ml with water. We then added a 0.5 ml aliquot of hydrofluoric acid to precipitate lanthanum fluoride, which carried the rare earths. We filtered and washed this precipitate with a cold solution of 2*M* HCl and 2*M* HF and then dried it under a heat lamp before mounting it on an aluminum counting plate. The chemical yield for the rare earths in each sample, determined by comparison of the intensity of the 103 keV gamma ray of the ^{153}Gd tracer with a standard aliquot, was normally between 50% and 80%. Small amounts of scandium and bromine were often present in these samples, but these activities did not interfere with the cross-section determinations. Samples were ready for counting within 30 min after the end of irradiation.

We irradiated the gold-backed targets for 5—10 min and then rapidly dismounted them, taped them to aluminum counting plates, and transported them to the counting apparatus, arriving between 3 and 5 min after the end of each bombardment. We counted these samples directly for the short-lived terbium isomers. In all experiments, except those using the highest two projectile energies, the gamma rays associated with the terbium isomers (as well as those arising from the ^{22}Ne + ^{nat}Cl reaction) were more intense than those arising from the products of the interaction of ^{22}Ne with the gold target backing because of the Coulomb barrier. Binder[22] has measured the mass yield in the reaction of 252 MeV ^{20}Ne with a thick gold foil and has found a minimum in the reaction cross section for nuclides in the $A=150$ region. With the lower incident energies used in our work, it is expected that these products will be formed with an even lower cross section.[23] We therefore feel justified in assuming that only insignificant contributions to the terbium cross sections come from the interaction of ^{22}Ne with gold.

We counted chemical fractions and unseparated targets for gamma rays with Ge(Li) detectors equipped with pulse-height analyzers. We measured chemical fractions for three months after the end of each irradiation; we measured unseparated targets for only a few hours. We set the chemical fractions 5 cm from the detector face to eliminate the necessity of geometrical corrections for finite source size (approximately 2 cm in diameter); we placed unseparated targets between 10 and 20 cm from the detector to reduce the count rate. All gamma-ray measurements covered the energy region from 90 keV to 2.0 MeV, stored in 4000 channels. We determined the detector efficiencies and peak shapes as a function of photon energy at several different count rates with a mixed radionuclide standard source. We mounted the standard at the same distance from the detector as were the experimental samples; we adjusted the dead time with a hot ^{94}Nb source (703 and 871 keV gamma rays) that was placed at a variable distance outside the line between the detector and the standard.

We analyzed the gamma-ray spectra with the SAMPO code,[24,25] which used input peak shapes as a function of

photon energy and detector dead time to find and integrate the gamma-ray peaks. These peak areas were corrected for counting time and detector efficiency (also functions of dead time), and were sorted into decay curves. We then performed a weighted-least-squares analysis on each decay curve using fixed half-lives. Relevant decay data for the nuclides of interest are given in Table I (Refs. 16, 17, and 26).

We obtained the cross sections of $^{147}Tb^m$, $^{148}Tb^m$, $^{149}Tb^m$, $^{150}Tb^B$, and $^{152}Tb^m$ from measurements of the unseparated targets. We used the cross section of $^{152}Tb^m$ to correct the initial activity of $^{152}Tb^g$ (obtained from measurements of the chemical fractions) for feeding by internal transition during the irradiation; the residual $^{152}Tb^g$ activity was consistent with zero in each case. We obtained the cross sections of $^{149}Tb^g$, $^{150}Tb^A$, and ^{151}Tb (including $^{151}Tb^m$) from measurements of the chemical fractions. We did not observe activities of the low-spin species $^{147}Tb^g$ and $^{148}Tb^g$ in any of the irradiations. For the quoted ^{151}Tb cross sections, we assumed that most of the observed activity resulted from the decay of $^{151}Tb^m$ (see below).

The results of evaporation calculations (discussed below) indicate that the gadolinium activities produced in $^{133}Cs(^{22}Ne,pxn)$ reactions are formed with lower cross sections than the terbium activities of the same mass that are produced in $^{133}Cs(^{22}Ne,xn)$ reactions. Because most of the terbium cross section lies in the short-lived high-spin isomers, it was impossible to extract meaningful independent gadolinium cross sections. In all experiments, the activities due to ^{147}Gd were consistent in magnitude with those expected solely from the decay of $^{147}Tb^m$. We were able to observe activity due to ^{146}Gd, and have attributed the measured cross sections to ^{146}Tb.

We also observed activities due to ^{145}Eu, ^{146}Eu, ^{147}Eu, and ^{148}Eu. We determined the amount of feeding of ^{146}Eu and ^{147}Eu by the decay of ^{146}Gd and ^{147}Gd, respectively, by decay curve analysis. We corrected the initial activities of ^{145}Eu for the alpha decays of ^{149}Tb and $^{149}Tb^m$, and corrected ^{147}Eu for alpha decay from ^{151}Tb. The ^{145}Eu activity might also be expected to be fed by ^{145}Gd, but ^{145}Gd was not produced with an observable intensity in any of the experiments.

III. RESULTS AND DISCUSSION

A. Evaporation from the compound nucleus

The independent cross sections that we have measured in our experiments are listed in Table II and are plotted as excitation functions in Figs. 1 and 2. The excitation energy of the compound nucleus, E^*, is determined from the mid-target projectile energy and the known mass excesses.[27] The energy widths of the points are approximately 1 MeV (Ref. 20). Data plotted for ^{150}Tb and ^{149}Tb are sums of both isomers, when observed. Lines connecting the same nuclides at different energies serve only to guide the eye.

We have simulated the deexcitation of the ^{155}Tb compound nucleus using the evaporation code ALERT.[10] ALERT produces a complete fusion spin distribution using transmission coefficients for the fusion of each partial wave calculated from the optical model with a parabolic barrier.[28] The probability of emitting a given particle from a given state is calculated with the Hauser-Feshbach expression[29] using the level density expression of Lang,[30] yrast energies calculated from the rotating liquid drop model,[31] and the angular-momentum-dependent particle transmission coefficients (for deformed nuclei) arising from the optical model.[10] Deexcitation by fission accounts for only 3% of the reaction cross section in the $^{20}Ne+^{133}Cs$ system[15] at a compound nucleus excitation energy of 100 MeV; therefore, we did not allow fission to compete with proton, neutron, alpha particle, and dipole photon emissions in the calculation. In this way, we have avoided introducing extra parameters for the level density of the system as it fissions and for the height of the fission barrier at high spins. The proper values of these parameters and their interpretation are under some contention.[32] We derived the reaction Q value and the particle binding energies in each deexcitation product from experimentally justified mass excesses[27] and input them to the

TABLE II. Measured cross sections (mb) from $^{22}Ne + ^{133}Cs$.

	Projectile energy (MeV)					
Nuclide	92.6	102.8	113.8	123.9	134.9	145.0
$^{152}Tb^m$	34.6±2.3	9.1±1.1				
^{151}Tb	353±38	255±29	123±15	32±4	4.4±0.7	
$^{150}Tb^A$	21.6±3.9	11.4±2.2	1.8±0.4			
$^{150}Tb^B$	139.9±6.8	402±19	462±21	273±36	103±6	
^{149}Tb	0.59±0.27	4.9±0.9	5.11±0.92			
$^{149}Tb^m$		55.2±7.6	219±30	320±70	313±43	84±12
$^{148}Tb^m$			27.3±2.8	98±14	283±18	299±33
$^{147}Tb^m$			0.19±0.04[a]	7.4±1.0	57±12	94±13
^{146}Tb					1.90±0.44[a]	17±3[a]
^{148}Eu	18.0±1.5	25.0±2.2	18.1±1.8	7.73±0.69	5.55±0.67	6.45±0.71
^{147}Eu	7.7±1.3	42.0±8.0	82±17	96±18	50±12	46±12
^{146}Eu		3.59±0.75	25.2±3.8	90±8	123±12	123±12
^{145}Eu		0.54±0.21	1.63±0.37	14.2±1.8	56.4±8.0	105±15

[a]Determined from daughter nuclide.

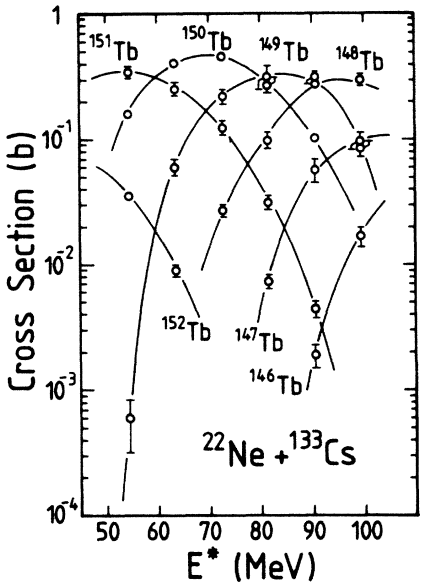

FIG. 1. Measured excitation functions of terbium activities produced in ^{133}Cs(^{22}Ne,xn)$^{155-x}$Tb reactions as a function of compound nucleus excitation energy. Data for ^{147}Tb and ^{148}Tb are for high spin isomers only. Lines connecting the points serve only to guide the eye.

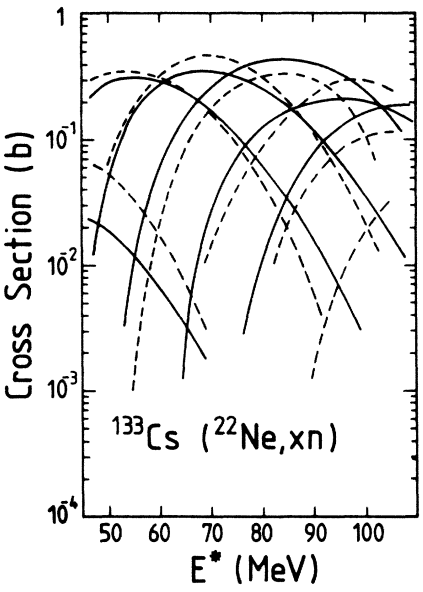

FIG. 3. Comparison of the experimental excitation functions (dashed lines) with the results of the evaporation calculation (solid lines) for ^{133}Cs(^{22}Ne,xn)$^{151-x}$Tb.

calculation. The level density ("little a") parameter was set to $a = A/12$ MeV^{-1}, which gave the best fit to the (CN,αxn)$^{151-x}$Eu activities.

Figures 3 and 4 show comparisons of the ALERT cross-section calculations (solid lines) with the experimental data (dashed lines). The available data on the relative isomer populations of ^{149}Tb and ^{150}Tb (Table II) seem to indicate that production of high-spin species dominates over that of low-spin species, and that the effect increases with the excitation energy (and angular momentum) of the compound nucleus. A similar result has been observed in the lower angular momentum ^{140}Ce(^{14}N,5n)^{149}Tb reaction.[33] Even though the ^{147}Tb and ^{148}Tb data plotted in Fig. 3 are for only the high-spin isomers of these nuclides, the total cross sections are unlikely to be significantly different. We will further justify this point later in this paper.

For the (CN,xn)$^{155-x}$Tb products, the positions and magnitudes of the cross-section maxima are well repro-

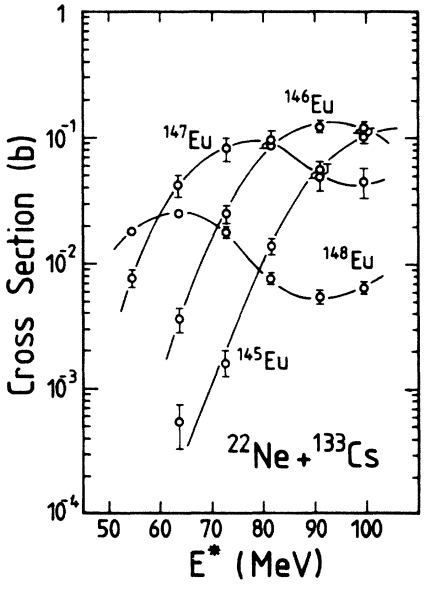

FIG. 2. Measured excitation functions of europium activities produced in ^{133}Cs(^{22}Ne,αxn)$^{151-x}$Eu reactions as a function of compound nucleus excitation energy. Lines connecting the points serve only to guide the eye.

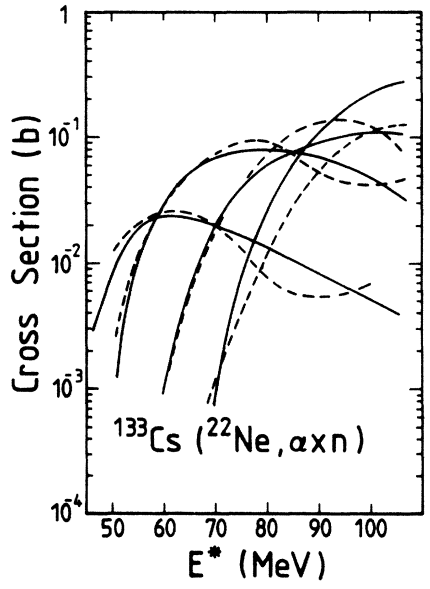

FIG. 4. Comparison of the experimental excitation functions (dashed lines) with the results of the evaporation calculation (solid lines) for ^{133}Cs(^{22}Ne,αxn)$^{151-x}$Eu.

duced by the calculation. The cross sections of the $(CN,\alpha xn)^{151-x}Eu$ products are also reproduced by the calculation, though structures at higher excitation energy are smoothed out. It should be noted that near $E^* = 100$ MeV there are losses from fission, which competes favorably with alpha-particle emission at high angular momentum.[10]

In the process of the cross-section calculations, ALERT produces the E-J distributions of the deexcitation products. Figure 5 shows the evolution of the E-J distribution through several selected products of four different reactions. Order-of-magnitude contours indicate the fraction of the total reaction cross section that passes through each 1 MeV by $1\hbar$ "box" of the E-J space of each product. Selected contours are labeled with the $\log_{10}$ of the cross section per box. Each compound nucleus E-J space contains an orthographic projection of the angular momentum distribution at constant excitation energy. A key to the units of the E-J space of each nuclide is shown in the upper left-hand corner of the figure.

The uppermost evaporation chain illustrates the deexcitation of ^{155}Tb produced in the reaction of 103 MeV ^{22}Ne with ^{133}Cs, which generates an excitation energy of 63 MeV in the compound nucleus. Successive evaporation of neutrons does not substantially reduce the angular momentum, as can be seen in the "settling" of the E-J population of the Tb products toward the yrast line. The population of products lying less than one neutron binding energy above this line deexcites further by gamma-ray emission to result in the products observed after the irradiation. Gamma-ray emission competes with particle emission in the deexcitation of the E-J population lying above this entry line.

Turning to the Eu isotopes produced in the reaction, it is clear that these may be produced in one of two ways: either by emission of an alpha particle and several neutrons, or by emission of two protons and the requisite number of neutrons. The two may be seen to lead to substantially different populations in the E-J plane, with energy maxima differing by the binding energy of the alpha particle.

It is well known that emission of an alpha particle leads to a longer evaporation chain and lower mass products. However, it is apparent from a study of the population in the E-J plane of a given nuclide, e.g., ^{150}Eu or ^{151}Eu, that emission of the more massive alpha particle actually leads to products with a higher average angular momentum than does the successive emission of protons and neutrons, due to the higher probability of alpha emission from high J (deformed) states.[10] Because the yrast line is concave upwards, subsequent emission of neutrons (following the alpha emission) leads to a more rapid encounter with the yrast line, thus somewhat shortening the evaporation chain. The net result is a reduction in the separation of product masses produced from evaporation by the two mass chains. In the deexcitation of 63 MeV ^{155}Tb*, where two proton evaporations are an unlikely event, this is not a particularly important effect. However, at higher excitation energies, the effect noticeably increases the yield of a given product from the multinucleon evaporation sequence.

The second set of E-J distributions in Fig. 5 also arises from the ^{22}Ne + ^{133}Cs reaction, but with higher projectile energy, producing ^{155}Tb with an excitation energy of 100 MeV. Populations arising from the two different evaporation chains (alpha emission or single particles) are even more clearly differentiated than in the lower energy case. A comparison of the contour diagrams also suggests several more subtle effects. At the lower energies, the Eu isotopes are produced almost exclusively following alpha emission; below mass 150, this mechanism accounts for most of the observed yield. At the higher energies, however, two-proton emission contributes significantly to the production of Eu nuclides. Species with lower average angular momentum and excitation energy are produced by the emission of four nucleons rather than by the emission of a single alpha particle (cf. peaks in the E-J contour plots for ^{150,151}Eu); the observed ^{148}Eu products are formed in greater yield by multinucleon evaporation than by evaporation chains containing an alpha particle emission. (This is deduced by integrating the separate contributions to the E-J space below the entry line.)

One goal of the detailed study of the evaporation chain as simulated by the ALERT code was to obtain information about the step at which alpha particle emission is most likely to occur. Early in the chain, when excitation energies and angular momenta are highest, increased deformation augments the probability of alpha emission relative to the other deexcitation processes. However, as the deexcitation proceeds and the yrast line is approached, competition from emission of other types of particles decreases and "type II" alpha particle emission,[34] akin to alpha emission from yrast trapping,[8] competes favorably with photon emission, resulting in a relative increase in the probability for this process. Roughly 7—8 % of excited ^{154}Tb evaporates an alpha particle, while roughly 13—15 % of ^{149}Tb does so. However, roughly 2.4 times the number of excited ^{154}Tb appear in the decay chain relative to ^{149}Tb. The two effects to some extent balance out. The question posed above must then be rephrased in less simplistic terms more relevant to what is observed in the laboratory: For a given observed product, e.g., ^{145}Eu, of a (HI,αxn) reaction, when was the alpha particle emitted? The answer may then be stated as follows.

The alpha particle emission occurs with somewhat larger absolute frequency early in the chain, but the decrease along the chain is not great. For the particular case illustrated in the center portion of Fig. 5, the decrease in yield from the second to the seventh evaporation step is only about 30%. Speculating further, for a lighter mass target-projectile system, Coulomb barrier effects enhance early alpha emission, whereas with a heavier mass target-projectile combination there may actually be an *increasing* amount of alpha emission along the chain.

The lowest two sets of evaporation chains shown in Fig. 5 depict the deexcitation of ^{151}Eu with $E^* = 100$ MeV, produced in the ^{18}O + ^{133}Cs and ^{12}C + ^{139}La reactions. Data from these systems have been reported previously.[18] The lighter projectile produces less angular momentum in the compound nucleus than does the heavier one, though the distribution of excitation energies integrated over angular momentum is essentially the same in the evapora-

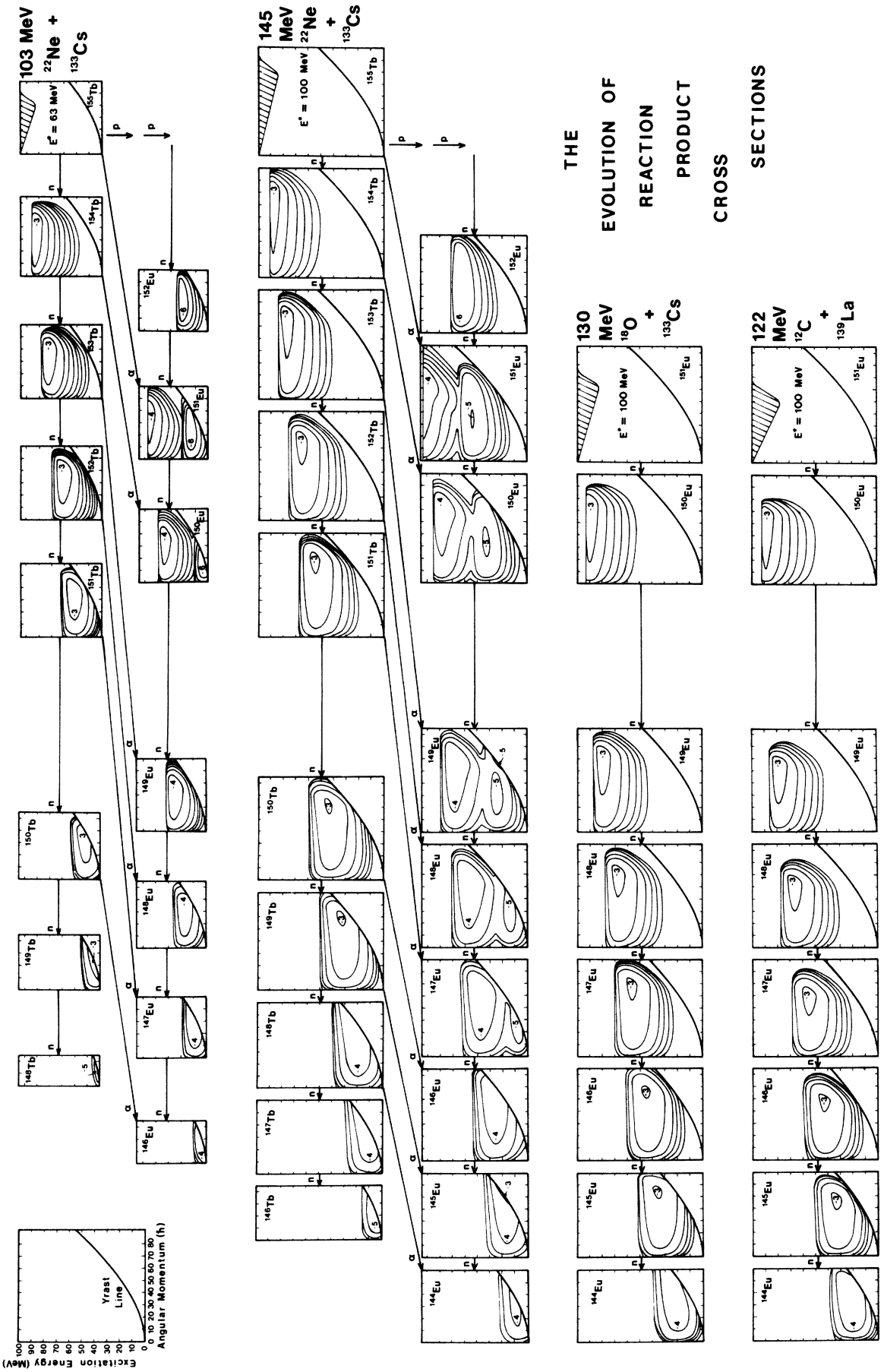

FIG. 5. The deexcitation of assorted complete fusion nuclei; populations of the excitation energy—angular momentum spaces of selected products. Contours are for orders of magnitude in the fraction of the total reaction cross section in each 1 MeV$\times 1\hbar$ unit. For further details, see text.

TABLE III. A comparison of the deposited angular momentum from the ALERT code and from Ref. 18.

	Reaction system			
	$^{133}Cs + {}^{18}O$		$^{139}La + {}^{12}C$	
E^* (MeV)	Ref. 18	ALERT	Ref. 18	ALERT
50.5	23.9	22.4	27.9	25.5
61.2	33.6	31.4	33.8	31.0
71.9	41.1	38.5	38.8	36.8
82.4	47.3	44.0	43.2	39.4
92.3	52.4	48.5	46.9	43.0

tion products of the two systems. This means that the E-J distribution produced by the heavier projectile reaches the yrast band before that produced by the lighter projectile; with the heavier projectile, a broadening of the excitation functions of the $(CN,xn)^{151-x}Eu$ products should be (and was) observed.

It is instructive to compare the $(CN,xn)^{151-x}Eu$ deexcitation products of the lower two systems with the $(CN,\alpha xn)^{151-x}Eu$ products of the second system, all arising from compound nuclei with $E^*=100$ MeV. The angular momentum distributions of the $^{133}Cs(^{22}Ne,\alpha xn)^{151-x}Eu$ products are similar to those arising from the evaporation of the same number of neutrons from $^{151}Eu^*$ produced in the $^{18}O + {}^{133}Cs$ reaction (a measure of the angular momentum removed by the alpha particle), but the upper edge of the excitation energy distribution is 15—20 MeV lower. It can therefore be expected that the peak cross section for products arising from the $^{133}Cs(^{22}Ne,\alpha xn)^{151-x}Eu$ process will be roughly two neutrons richer than that arising from the $^{133}Cs(^{18}O,xn)^{151-x}Eu$ process, starting from compound nuclei with the same excitation energy.

As mentioned above, ALERT calculates the spin distribution of the compound nucleus via the optical model. We compare the root-mean-square angular momentum deposited in the compound nucleus with the l_{crit} values derived from the experimental data by the semiclassical Diamond-Stephens approach[35] reported in Ref. 18. It is to be expected that the rms values would be slightly lower than those for l_{crit} but follow the same trend. This is indeed what is observed. (See Table III.)

B. Isomer ratios

The portion of the E-J distribution that lies too close to the yrast line to undergo further particle evaporation is considered to deexcite primarily by photon emission, resulting in the evaporation residues for the particular nuclides in which it resides. It is this part of the deexcitation process which determines the relative population of isomeric states. Rather than determine spin cutoff parameters[33,36] which reproduce the isomer ratios, we have attempted to derive the isomer ratios *a priori* using an approach similar to that of Groening *et al.*[13,14]

The E-J population for a particular nuclide is "trimmed" of all the cross section that continues along the evaporation chain via particle emission; the residual is input into the computer code MUBEAR, in which the gamma-ray deexcitation process is simulated. These data consist of a population matrix of cross section per unit excitation energy per unit angular momentum, the spin of each bin, and the upper extreme of its excitation energy. This "bin format" is not compatible with nuclear levels, so the data are converted to "level format" as follows: The energy of the number-average level of each box is determined numerically from the level density expression of Lang,[30]

$$\rho(E,J)\propto[E-B(J)]^{-2}\exp(2\{a[E-B(J)]\}^{1/2}), \quad (1)$$

where E is the excitation energy, J is the spin, a is the level density parameter (maintained at $a=A/12$ MeV^{-1}, as before), and $B(J)$ is the energy of the yrast line at spin J. All of the energy levels associated with each particular box are assumed to reside at this average energy value; the absolute number of these levels is determined by numerically integrating the normalized $\rho(E,J)$ over the energy limits of the box. The normalization constant N_0 is, roughly,[37]

$$N_0=\frac{2J+1}{12}a^{1/2}\left[\frac{B(J)}{J(J+1)}\right]^{3/2}. \quad (2)$$

In the ALERT calculation, which provides the input E-J populations, no special provision is made for half-integral spins (odd mass nuclei); for odd A nuclei, MUBEAR assumes that bins labeled with $J=0$ are really $J=\frac{1}{2}$, that $J=1$ boxes are really $J=\frac{3}{2}$, etc. ALERT also makes no attempt to keep track of parity; MUBEAR divides each bundle of levels in half, assigns to these halves opposite parities, and splits the cross section of their parent box equally between them.

MUBEAR takes as further input the known discrete energy levels and their spins and parities for each nuclide considered for an isomer calculation. These levels are placed among the calculated levels, which are modified as follows: Because the known discrete levels at a particular value of J^π are almost always among the lowest in energy, the code assumes that inclusion of discrete levels at a particular J^π value is cause for removal of a similar number of levels from the lowest energy bundle at that J^π. If there are not enough calculated levels in that bundle, the next bundle at that J^π loses levels. The cross-section populations of the resulting level scheme are determined by dividing up the cross section present in the original bundle between the discrete levels and the new bundle according to their number densities.

The transition rate for the emission of gamma rays of multipolarity l between states that are neither strictly single particle nor collective in nature is, approximately,[13,38,39]

$$T_{if} \propto |M_{if}(\sigma l)|^2 n_f E_\gamma^{2l+1} , \quad (3)$$

where n_f is the number of states in the receiving bundle, E_γ is the transition energy, and $M_{if}(\sigma l)$ is the reduced transition matrix element. Groening *et al.*[13] determined that the best results for ^{44}Sc were obtained with

$$\frac{|M_{if}(E2)|^2}{|M_{if}(E1)|^2+|M_{if}(M1)|^2} = \frac{3}{97} . \quad (4)$$

Starting with the populated bundle of states at highest excitation energy and angular momentum, MUBEAR calculates the relative rates for $E1$, $M1$, and $E2$ gamma transitions to each bundle allowed by the selection rules. These rates are normalized against the total rate for depopulating the initial bundle, and the cross section for the bundle is distributed among the final states accordingly. This procedure is performed for each bundle until only the isomeric states are still populated.

Unfortunately, the level schemes of the neutron-deficient terbium nuclides are not well known. As a result, the only discrete states that have been input into the calculations are the two isomeric states of each nuclide, whose excitation energies (small relative to the 1 MeV box size) were set equal to zero. We found that changing the admixture of $E2$ gamma rays, introduced via the $M_{if}(E2)$ parameter, had very little effect on the isomer ratios resulting from the calculation. This is not an unexpected result; from Fig. 5 we know that the vast majority of the reaction cross section lies in states with significantly higher angular momenta than the isomeric states, so regardless of the $E2$ admixture, the bulk of the cross section reaches the yrast line before it decays as far as the isomeric states.

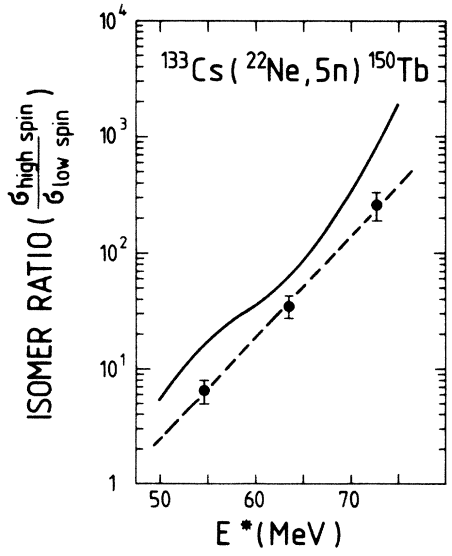

FIG. 6. Comparison of the calculation (solid line) with the experimental data for the isomer ratio of ^{150}Tb as a function of compound nucleus excitation energy.

A typical result is shown in Fig. 6 for the ^{133}Cs(^{22}Ne,5n)^{150}Tb reaction. The trend of the experimental data is well reproduced by the calculation (solid line), but the calculated isomer ratios are uniformly high by a factor of 3. We attribute this to the lack of information about low-lying nuclear levels in the vicinity of the high-spin isomer. The isomer ratio is such a large number that passage of even a minute fraction of the cross section bound for the high-spin state into the angular momentum region between the two isomers has a drastic effect on the isomer ratio; this passage can be accomplished via nuclear structure near the high-spin isomer. Presumably the $E2$ admixture becomes more critical to the calculations as more nuclear level information becomes available. The calculated isomer ratios for the other terbium nuclides show a similar behavior to that of ^{150}Tb, rising from roughly 10 near the threshold energy to between 200 and 1000 near the excitation function maxima.

IV. CONCLUSIONS

We have measured the excitation functions for several of the products of the deexcitation of the complete fusion nucleus ^{155}Tb, produced in the ^{22}Ne + ^{133}Cs reaction. We have been able to reproduce these data with the evaporation code ALERT.[10] The ^{133}Cs(^{22}Ne,xn)$^{155-x}$Tb cross sections result almost entirely in the production of the high-spin isomers of these nuclides. The ^{133}Cs(^{22}Ne,αxn)$^{151-x}$Eu cross sections show structure at high reaction energies caused by contributions from the (CN,2p(x+2)n)$^{151-x}$Eu process.

The isomer ratios of the terbium nuclides have been calculated using a new code, MUBEAR, from the E-J distributions arising from the evaporation calculation. The calculated isomer ratios are only weakly dependent on the admixture of $E2$ multipolarity gamma rays in the deexcitation caused by the high angular momenta of the emitting systems. Our calculation overestimates the isomer ratios, probably due to a lack of information about the level schemes of the products.

ACKNOWLEDGMENTS

We would like to thank the staff and crew of the Lawrence Berkeley Laboratory 88-in. cyclotron for quickly and efficiently providing the ^{22}Ne beams used in this work. The interest and support of G. T. Seaborg is greatly appreciated. M. Blann not only made his computer code ALERT available to us, but also made many important and helpful suggestions. We would also like to thank H. Groening and W. Westmeier for several interesting discussions. One of the authors (K.J.M.) would like to acknowledge the hospitality of the Lawrence Berkeley Laboratory and the Gesellschaft für Schwerionenforschung during most of this work. This work was performed under the auspices of the U.S. Department of Energy, under Contract No. De-AC03-76SF00098, and by the Lawrence Livermore National Laboratory of the U.S. Department of Energy under Contract No. W-7405-Eng-48.

[1]M. Lefort, J. Phys. (Paris) Colloq. **5**, C-57 (1976).
[2]P. E. Hodgson, *Nuclear Heavy Ion Reactions* (Clarendon, Oxford, 1978), Chap. 4.
[3]J. R. Grover, Phys. Rev. **127**, 2142 (1962).
[4]J. R. Grover and J. Gilat, Phys. Rev. **157**, 802 (1967).
[5]M. Blann, Phys. Rev. **157**, 860 (1967).
[6]J. R. Grover, Phys. Rev. **157**, 832 (1967).
[7]J. R. Grover and J. Gilat, Phys. Rev. **157**, 814 (1967).
[8]J. R. Grover and J. Gilat, Phys. Rev. **157**, 823 (1967).
[9]M. Blann and F. Plasil, Phys. Rev. Lett. **29**, 303 (1972).
[10]M. Blann, Phys. Rev. C **21**, 1770 (1980).
[11]G. Rudstam, Phys. Scr. **20**, 165 (1979).
[12]I. S. Grant and M. Rathle, J. Phys. G **5**, 1741 (1979).
[13]H. Groening, K. Aleklett, K. J. Moody, P. L. McGaughey, W. Loveland, and G. T. Seaborg, Nucl. Phys. **A389**, 80 (1982).
[14]H. Groening, K. J. Moody, and G. T. Seaborg, Nucl. Instrum. Methods **214**, 317 (1983).
[15]F. Plasil, R. L. Ferguson, R. L. Hahn, F. E. Obenshain, F. Pleasonton, and G. R. Young, Phys. Rev. Lett. **45**, 333 (1980).
[16]*Table of Isotopes,* edited by C. M. Lederer and V. S. Shirley (Wiley, New York, 1978).
[17]J. J. Hogan, Radiochim. Acta **27**, 73 (1980).
[18]J. J. Hogan, Z. Phys. A **299**, 163 (1981).
[19]K. E. Gregorich, K. J. Moody, and G. T. Seaborg, Radiochim. Acta **35**, 1 (1984).
[20]F. Hubert, A. Fleury, R. Bimbot, and D. Gardes, Ann. Phys. (Paris) **5**, 1 (1980).
[21]L. C. Northcliffe and R. F. Schilling, Nucl. Data Tables **7**, 233 (1970).
[22]I. Binder, Ph.D. thesis, Lawrence Berkeley Laboratory Report No. LBL-6526, 1977 (unpublished).
[23]H. Kudo, K. J. Moody, and G. T. Seaborg, Phys. Rev. C **30**, 1561 (1984).
[24]J. T. Routti and S. Prussin, Nucl. Instrum. Methods **72**, 125 (1969).
[25]D. J. Morrissey, D. Lee, R. J. Otto, and G. T. Seaborg, Nucl. Instrum. Methods **158**, 499 (1979).
[26]U. Reus and W. Westmeier, At. Data Nucl. Data Tables **29**, 1 (1983).
[27]A. H. Wapstra and K. Bos, At. Data Nucl. Data Tables **19**, 177 (1977).
[28]T. D. Thomas, Phys. Rev. **116**, 703 (1959).
[29]R. Bass, *Nuclear Reactions with Heavy Ions* (Springer-Verlag, Berlin, 1980), Chap. 8.
[30]D. W. Lang, Nucl. Phys. **77**, 545 (1966).
[31]S. Cohen, F. Plasil, and W. J. Swiatecki, Ann. Phys. (N.Y.) **82**, 557 (1974).
[32]M. Blann, Phys. Rev. Lett. **49**, 505 (1982).
[33]J. M. Alexander and G. N. Simonoff, Phys. Rev. **130**, 2383 (1963).
[34]A. Fleury, H. Delagrange, and J. P. Dufour, Phys. Rev. C **16**, 1396 (1977).
[35]P. O. Tjom, F. S. Stephens, R. M. Diamond, J. de Boer, and W. E. Meyerhof, Phys. Rev. Lett. **29**, 303 (1972).
[36]G. Liggett and D. Sperber, Phys. Rev. C **3**, 447 (1971).
[37]A. Bohr and B. R. Mottelson, *Nuclear Structure* (Benjamin, New York, 1969), Vol. 1, p. 155.
[38]R. M. Diamond and F. S. Stephens, Annu. Rev. Nucl. Part. Sci. **30**, 85 (1980).
[39]R. J. Liotta and R. A. Sorenson, Nucl. Phys. **A297**, 136 (1978).